Draft version 2.0

ATLAS NOTE

January 14, 2008

ATL-PHYS-CONF-2008-003

18 January 2008

Search for Low-Scale Technicolor in ATLAS

G. Azuelos[1],[2], J. Ferland[1], K. Lane[3] and A. Martin[4]

[1]Université de Montréal
[2]TRIUMF,Vancouver
[3]Boston University
[4]Yale University

Abstract

Low scale technicolor is an appealing scenario of strong electroweak symmetry breaking. It has a rich phenomenology which can be tested at the LHC. A very characteristic signal would involve the observation of a technipion in resonance with a Standard Model gauge boson. A fast simulation analysis of the process $pp \to \rho_T^\pm \to \pi_T^\pm Z \to bj\ell\ell$ and $pp \to a_T^\pm \to \pi_T^\pm Z \to bj\ell\ell$ for three representative sets of masses for the new particles suggests that the technirho and technipion could be observed with ~ 15 fb^{-1}, and that the a_T could be observed simultaneously with the ρ_T and π_T within a year or more of running at the LHC.

1 Introduction

Understanding the mechanism of electroweak symmetry breaking is the foremost goal of the LHC. It will probe the TeV scale where, in the absence of light Higgs boson or other such mechanism, perturbative unitarity would be violated in the scattering of longitudinally-polarized electroweak bosons (generically, W_L). Hence, the famous "no-lose theorem" [1] that implies the LHC will uncover the origin of electroweak symmetry breaking whatever it may be.

Technicolor (TC) [2, 3] is an appealing scenario of electroweak symmetry breaking. In TC, a strong, vector-like gauge interaction of massless technifermions causes their chiral symmetry to be spontaneously broken. If these technifermions transform under $SU(2) \otimes U(1)$ as quarks and leptons do, this effect also breaks electroweak gauge symmetry down to electromagnetic $U(1)$. Modern technicolor has a slowly-running ("walking") gauge coupling [4–7]. This feature allows extended technicolor (ETC) [8] to generate realistic masses for quarks, leptons and technipions (π_T) with the very massive (10^3–10^4 TeV) ETC bosons necessary to suppress flavor-changing neutral current interactions. (For reviews, see Refs. [9, 10].) The important phenomenological consequence of walking is that the technicolor scale is likely to be much lower and the spectrum of this low-scale technicolor (LSTC) much richer and more experimentally accessible than originally thought [11–13]. The reason for this is that many technifermion doublets are required to make the TC coupling walk. The bound states of the lightest technifermion doublet, spin-one $\rho_T^{\pm,0}$ and ω_T and spin-zero $\pi_T^{\pm,0}$, will all be accessible at the LHC. Furthermore, walking enhances π_T masses much more than those of their vector partners, ρ_T and ω_T, closing the all-π_T decay channels of these lightest techni-vectors. In LSTC, then, we expect the lightest ρ_T and ω_T to lie below roughly 0.5 TeV and to be very narrow — because they decay predominantly to an electroweak boson γ, W, Z plus π_T or to a pair of electroweak bosons. These channels have very distinctive signatures, made all the more so because ρ_T and ω_T are narrow, $\Gamma(\rho_T) \simeq 1$–$5\,\text{GeV}$ and $\Gamma(\omega_T) \simeq 0.1$–$0.5\,\text{GeV}$. Technipions are expected to decay via ETC interactions to the heaviest fermion-antifermion flavors allowed kinematically, providing the best chance of their being detected.[1)]

It has been argued [15, 16] that walking TC invalidates the standard QCD-based calculations of the precision-electroweak S-parameter [17–20]. Walking TC produces something like a tower of vector *and axial-vector* isovector states above the lightest ρ_T and its axial partner a_T, and they all may contribute significantly to the S-parameter.[2)] Most important phenomenologically, in models with small S, the lightest a_T and ρ_T are likely to be nearly degenerate and have similar couplings to their respective weak vector and axial-vector currents; see, e.g., Refs. [21–24]. The $a_T \to 3\pi_T$ modes are closed and they too are very narrow, $\Gamma(a_T) \lesssim 0.5$ GeV.

The phenomenology of these technihadrons is set forth in the "Technicolor Straw-Man Model" (TCSM) [24–26]. The principal LSTC discovery channels at the Tevatron, $\rho_T \to W^\pm \pi_T^{\mp,0} \to \ell^\pm \nu_\ell b\text{j}$, are swamped by $\bar{t}t$ production at the LHC. There, the discovery modes are most probably $\rho_T^\pm \to W^\pm Z^0$, $\omega_T \to \gamma Z^0$ and $a_T^\pm \to \gamma W^\pm$, with leptonic (e and/or μ) decay modes for W and Z. These modes do not involve technipions, an essential feature of low-scale technicolor. There are other strong-interaction scenarios of electroweak symmetry breaking (so-called Higgsless model in five dimensions and deconstructed models, to name two examples) which predict narrow vector and axial-vector resonances, but they do not decay to technipion-like objects. Therefore, observation of technipions is important for confirming LSTC as the mechanism underlying electroweak symmetry breaking. Thus motivated, we evaluate here the observability of the process $pp \to \rho_T^\pm / a_T^\pm \to Z^0 \pi_T^\pm \to \ell^+ \ell^- b j$ which, at the LHC, is much less dominated by background than the $W\pi_T$ channels. An attractive feature of this process is the possibility of discovering ρ_T and a_T peaks in the same $Z\pi_T$ final state. We find this can be done in a

---

[1)] Something like topcolor-assisted technicolor [14] is needed to keep the top quark from decaying copiously into $pi_T^+ b$ when $M_{\pi_T} \lesssim 160$ GeV. Thus, if π_T^+ is heavier than the top, it will not decay exclusively to $t\bar{b}$.

[2)] These higher mass states are also important in unitarizing longitudinal gauge boson scattering at high energies.

$100\,\text{fb}^{-1}$ data sample except at the highest masses we consider, $\sim 600\,\text{GeV}$, where only the ρ_T peak is significant.

2 Signal and backgrounds

The process of production and decay of charged techni-rhos of the TCSM is implemented in PYTHIA [27], version 6.411. In order to account for new processes involving the a_T, as discussed in the introduction, the relevant subroutines were replaced by revised versions, provided by S. Mrenna [28]. Three different reference cases labeled A, B and C were considered, for which Table 1 summarizes the basic parameters. The processes $Z_\perp \pi_T^\pm$ and $Z_L \pi_T^\pm$ are both included. Both $\rho_T^\pm$ and $a_T^\pm$ contribute to the production of transversely-polarized $Z_\perp$ while only $\rho_T^\pm$ contribute to longitudinally-polarized Z production. A choice of mass for some techniparticles is shown, as well as for the parameters M_V, M_A, which control the strength of the technivector decay to a technipion and a transversely polarized electroweak boson. We also used $Q_U = 1$ and $Q_D = 0$ for technifermions charges. The other parameters of TCSM are those by default in PYTHIA. The main ones are: number of technicolors $N_{TC} = 4$ and mixing angle between interaction eigenstates of technipion and vector bosons $\sin\chi = 1/3$.

Various backgrounds will contribute : $t\bar{t}$, Zjj, Zbj and $Zb\bar{b}$. The sample $t\bar{t}$ has been generated with PYTHIA allowing the top quark and W bosons to decay freely. The process $Zb\bar{b}$ was generated by AcerMC [29] 3.4 while Zjj and Zbj are from MadGraph [30] 4.1.33. Z+jets events were produced using partons distribution function(pdf) CTEQ6L and a renormalization and factorization scale Q at the Z boson mass. The sample Zjj does not include $Zb\bar{b}$, but there may be double counting of Zjj and Zbj for low p_T jets. These Z+jets events were then processed by PYTHIA for hadronization and fragmentation. The background cross sections shown in Table 2 have been multiplied by the branching ratio ($BR(Z \to ll)$), except for $t\bar{t}$, where no decay channel was imposed. It must be noted that all signal and background cross sections quoted here are at leading order. The K factors can be substantial (~ 1.5).

Table 1: Parameters used for producing signal samples.

Sample	M_{ρ_T},M_{ω_T},Λ_{V_T}, Λ_{A_T} [GeV]	M_{a_T} [GeV]	M_{π_T} [GeV]	$M_{\pi'_T}$ [GeV]	σxBR [fb]	
					ρ_T	a_T
A	300	330	200	400	98.7	58.9
B	400	440	275	500	71.2	17.4
C	500	550	350	600	36.5	8.9

Table 2: Background cross-sections at leading order. No branching ratio is applied to the $t\bar{t}$ background.

Bkg	$\sigma xBR(Y \to ll + X)$ [pb]
$t\bar{t}$	500.0
Zjj	344.0
Zbj	11.0
$Zb\bar{b}$	56.0

The ATLAS detector simulation for signals and backgrounds was performed using the ATLFAST [31, 32] implemented in the ATLAS software framework ATHENA, version 12.0.7. It is a good approximation of detector resolution and efficiency, and is fast enough to process the large number of events. An additional efficiency factor of 10% has been applied for lepton identification inefficiency. The b-jet tag efficiency used was 60% with corresponding global mistagging factors of ∼1% for light-quark jets and gluon jets and of ∼10% for c-jets. The exact rejection factors depend on the reconstructed jet p_T and η.

3 Analysis

In order to satisfy the trigger conditions, and considering that high luminosity running conditions would apply, we require as a preselection a minimal set of criteria: (i) the presence of two same-flavour and opposite sign leptons with $p_T > 20$ GeV and (ii) at least one b-tagged jet and one non-b-tagged jet, both with $p_T > 20$ GeV. The two jets with highest p_T satisfying these conditions will be the candidate jets resulting from the technipion decay.

On these preselected events, we apply several selection criteria to increase the significance of the signal with respect to the backgrounds. Figure 1, normalized to 100 fb^{-1}, justifies the set of cuts used:

- **cut 1:** Since the signal leads to no significant missing energy, we can strongly suppress the $t\bar{t}$ background, as shown in 1(a), by imposing

$$E_T^{miss} < 35 \text{ GeV}$$

- **cut 2:** The jets associated to the $\pi_T^{\pm}$ will have greater transverse momentum for the signal than for backgrounds, due to their physical origin and the event topologies. Figure 1(b) shows the distribution for the highest-p_T jet. The optimal cut for case A was found to be

$$p_T^{max}(j,b) > 80 \text{ GeV}$$

  This cut varies with the $\pi_T^{\pm}$ mass. It was found that values of 115 GeV and 150 GeV for samples B and C respectively were optimal selection criteria.

- **cut 3:** Figure 1(c) shows the distribution for the lower-p_T jet. We require for sample A:

$$p_T^{min}(j,b) > 65 \text{ GeV}$$

  As for cut 3, the dependence of the value depend on the $\pi_T^{\pm}$ mass. Values of 80 GeV and 100 GeV were found to be optimal for case B and C respectively. When analysing real data, a scan of assumed mass points would be considered and this cut and cut 4 below would be ajusted accordingly.

- **cut 4:** Since only one b-jet is expected from the decay of the $\pi_T^{\pm}$, whereas the $t\bar{t}$ background will produce two such jets, we impose a cut:

$$\text{number of b-tagged jets} = 1$$

- **cut 5:** Finally, the requirement that the two opposite sign, same flavor leptons should have an invariant mass close to the Z mass should further suppress the $t\bar{t}$ background:

$$m_{\ell\ell} = 91 \pm 5 \text{GeV}$$

The same analysis has been repeated, optimizing for the search of the a_T only. It was found that a better significance for its discovery could be obtained by replacing cuts 2 and 3 by: $p_T^{max}(j,b) > 85$ GeV, 120 GeV and 180 GeV and $p_T^{min}(j,b) > 50$ GeV, 80 GeV and 90 GeV for the three cases under study.

Tables 3, 4 and 5 give the number of signal and background events remaining in the peak region as the cuts are successively applied. The region is chosen as an ellipse centered at the mean while the widths correspond to 1.5 sigma interval.

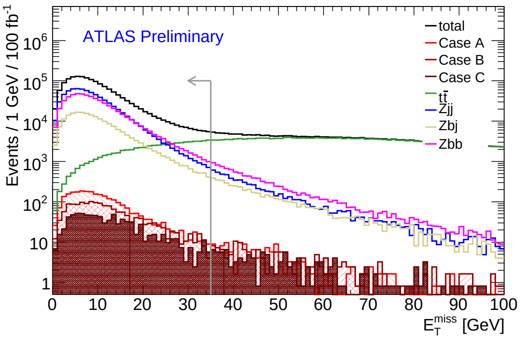

(a) Missing transverse energy

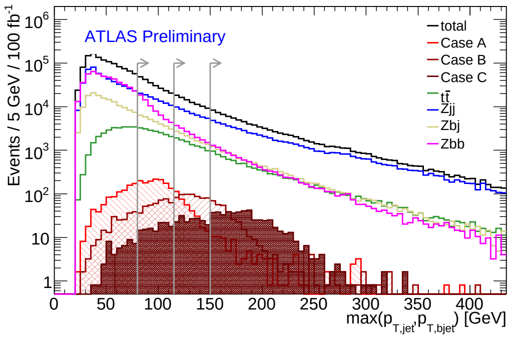

(b) Transverse momentum of the hardest jet used in the $\pi_T^{\pm}$ reconstruction

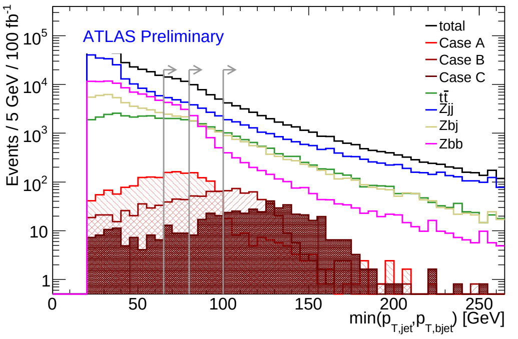

(c) Transverse momentum of the lower p_T jet used in the $\pi_T^{\pm}$ reconstruction

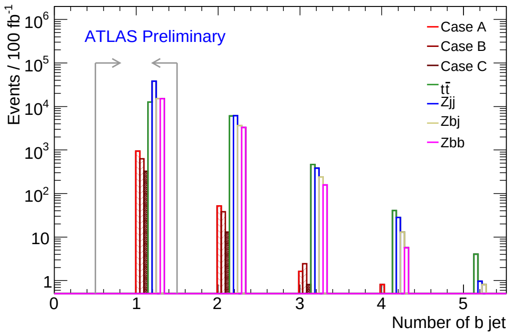

(d) Number of b jets with $p_T > 20$ GeV.

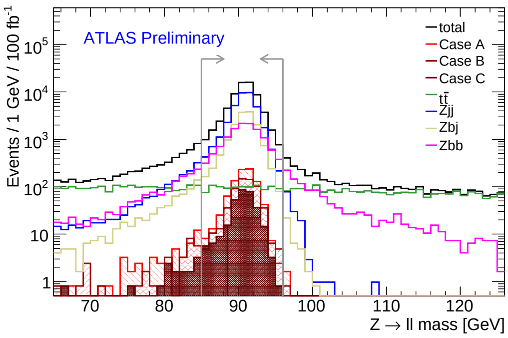

(e) Invariant mass of the two leptons

Figure 1: Set of cuts used to suppress backgrounds

Table 3: Case A: Event flow in function of cuts applied. S stands for the number of signal events in the peak regions, while B is the number of background for the same region, normalized to 100 fb^{-1}.

Cut	peak	S	$t\bar{t}$	Zjj	Zbj	$Zb\bar{b}$	B	$\frac{S}{\sqrt{B}}$	$\frac{S}{\sqrt{S+B}}$
initial	$\rho_T^\pm$	548	1521	2269	694	2442	6927	6.6	6.4
	$a_T^\pm$	297	2372	3665	1164	3472	10672	2.9	2.9
after cut1	$\rho_T^\pm$	548	281	2257	677	2413	5629	7.3	7.0
	$a_T^\pm$	295	463	3638	1133	3413	8648	3.2	3.1
after cut2	$\rho_T^\pm$	431	215	512	209	279	1217	12.4	10.6
	$a_T^\pm$	251	339	1106	385	602	2432	5.1	4.9
after cut3	$\rho_T^\pm$	362	144	239	125	130	640	14.3	11.4
	$a_T^\pm$	226	279	518	271	330	1398	6.0	5.6
after cut4	$\rho_T^\pm$	347	107	203	102	112	525	15.1	11.8
	$a_T^\pm$	215	204	449	215	272	1140	6.4	5.8
after cut5	$\rho_T^\pm$	344	19	190	96	97	403	17.1	12.6
	$a_T^\pm$	215	19	431	207	243	900	7.2	6.4

Table 4: Case B: Event flow in function of cuts applied. S stands for number of signal events in the peak regions, while B is the number of background for the same region, normalized to 100 fb^{-1}.

Cut	peak	S	$t\bar{t}$	Zjj	Zbj	$Zb\bar{b}$	B	$\frac{S}{\sqrt{B}}$	$\frac{S}{\sqrt{S+B}}$
initial	$\rho_T^\pm$	382	1785	2376	801	2539	7503	4.4	4.3
	$a_T^\pm$	117	1791	2049	666	1777	6283	1.5	1.5
after cut1	$\rho_T^\pm$	380	319	2356	773	2477	5926	4.9	4.8
	$a_T^\pm$	113	350	2023	637	1712	4722	1.6	1.6
after cut2	$\rho_T^\pm$	295	169	426	175	147	918	9.7	8.5
	$a_T^\pm$	96	170	455	179	156	960	3.1	3.0
after cut3	$\rho_T^\pm$	262	137	224	133	71	537	11.3	9.3
	$a_T^\pm$	79	118	171	90	41	419	3.9	3.5
after cut4	$\rho_T^\pm$	248	97	196	107	67	448	11.7	9.4
	$a_T^\pm$	75	76	480	66	37	328	4.1	3.7
after cut5	$\rho_T^\pm$	242	15	185	105	56	346	13.0	10.0
	$a_T^\pm$	75	3.2	143	65	32	242	4.8	4.2

Table 5: Case C: Event flow in function of cuts applied. S stands for number of signal events in the peak regions, while B is the number of background for the same region, normalized to 100 fb^{-1}.

Cut	peak	S	$t\bar{t}$	Zjj	Zbj	$Zb\bar{b}$	B	$\frac{S}{\sqrt{B}}$	$\frac{S}{\sqrt{S+B}}$
initial	$\rho_T^\pm$	184	880	965	292	878	3016	3.4	3.3
	$a_T^\pm$	35	828	805	258	659	2550	0.7	0.7
after cut1	$\rho_T^\pm$	182	149	952	274	855	2232	3.9	3.7
	$a_T^\pm$	35	133	789	247	639	1808	0.8	0.8
after cut2	$\rho_T^\pm$	148	63	135	52	35	286	8.8	7.1
	$a_T^\pm$	23	32	95	28	22	177	1.7	1.6
after cut3	$\rho_T^\pm$	133	46	65	32	15	159	10.7	7.8
	$a_T^\pm$	21	23	49	23	11	106	2.0	1.9
after cut4	$\rho_T^\pm$	127	27	59	24	15	126	11.4	8.0
	$a_T^\pm$	21	11	43	17	11	82	2.3	2.1
after cut5	$\rho_T^\pm$	126	2.4	58	23	12	96	13.0	8.5
	$a_T^\pm$	21	1.6	42	17	8.9	69	2.5	2.2

The resolution of the $\pi_T^\pm$,$\rho_T^\pm$ and $a_T^\pm$ reconstruction is about 15 GeV (see Fig. 2(a) and 2(b)). Because of correlated reconstruction resolutions of the ρ_T/a_T and π_T, the difference in mass will have a better resolution (see Fig. 2(c)). This is what is plotted in one of the axes of Fig. 3 where the observed signal for case A is shown for an integrated luminosity of 100 fb^{-1}. Figure 3(a) shows the technicolor signal only while fig. 3(b) shows the background. The sum of both, shown on fig. 3(c), displays clearly two peaks, which have a significance of 17 and 7 and containing 344 and 160 events of the signal.

Cases B and C have similar behavior and are not shown. The cross section times BR required for a 5-σ discovery at 100 fb^{-1} is given in Table 6 for each of the three cases studied here. Table 7 shows the needed luminosity in fb^{-1} for a 5-σ discovery.

Table 6: Minimal cross-section multiply by branching fraction needed to obtain a significance of five for each case studied for the $\rho_T^\pm/a_T^\pm$ signal at 100 fb^{-1}.

Sample	peak	A	B	C
σxBR [fb]	$\rho_T^\pm$	28.5	27.6	14.0
	$a_T^\pm$	40.6	17.9	17.6

Table 7: Minimal luminosity needed to obtain a significance of five for each case studied

Sample	peak	A	B	C
Luminosity [fb^{-1}]	$\rho_T^\pm$	8.3	15.1	14.8
	$a_T^\pm$	47.5	106	390

As mentioned in sect. 2, the results shown here do not account for NLO corrections of background or signal cross section. It is known that they could be of the order of 50% and, for $t\bar{t}$ in particular (which is not the dominant background), it reaches 66%. The significance of the signal can therefore be assigned an uncertainty of $\sim$25%

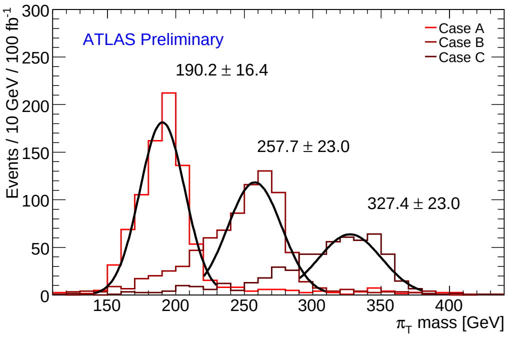

(a) Reconstructed masses of the π_T for the three signal cases.

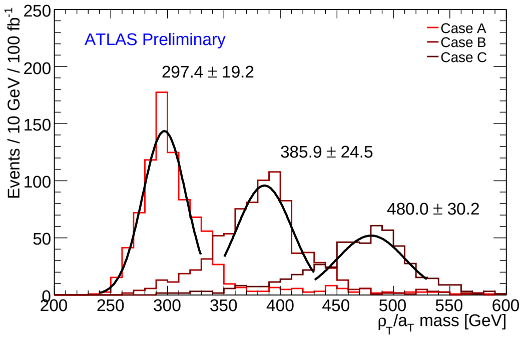

(b) Reconstructed masses of the ρ_T for the three signal cases.

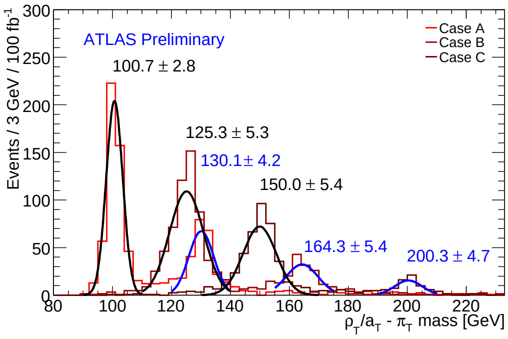

(c) Reconstructed mass differences $M_{\rho_T} - M_{\pi_T}$ and $M_{a_T} - M_{\pi_T}$ for the three signal cases.

Figure 2: Reconstructed mass resolution for signals.

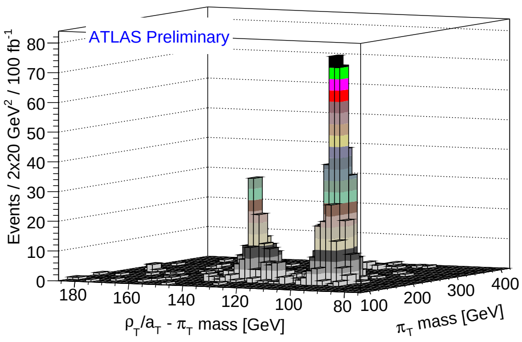

(a) π_T mass as function of (ρ_T/a_T-π_T) mass for case A signal.

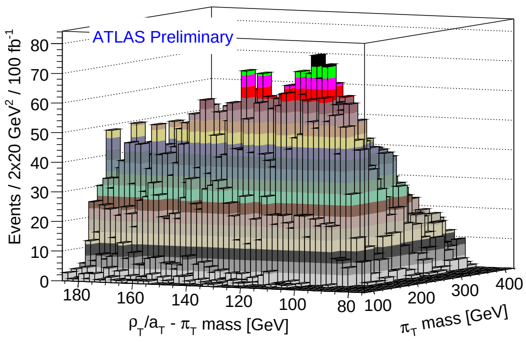

(b) π_T mass as function of (ρ_T/a_T-π_T) mass for backgrounds only.

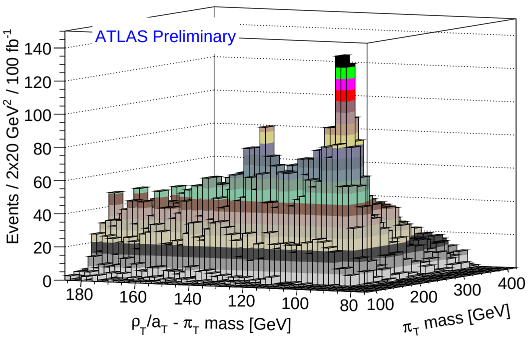

(c) π_T mass as function of (ρ_T/a_T-π_T) mass for sum of case A signal and backgrounds.

Figure 3: π_T mass as function of (ρ_T/a_T-π_T). The selection criteria applied here are those optimized for the ρ_T resonance.

4 Summary and conclusion

As a test of TCSM model, the process $pp \rightarrow \rho_T^{\pm}/a_T^{\pm} \rightarrow Z\pi_T^{\pm} \rightarrow \ell\ell\ bj$ is an important signal to be investigated at the LHC since it involves clearly three(ρ_T, a_T and π_T) resonances. It also provides a measure of the coupling of these resonances to vector bosons. However, the signal presents experimental challenges because of large backgrounds. From an analysis based on simple selection cuts for three reference cases in parameter space, we have found that there is a strong potential for observing the ρ_T with an integrated luminosity of 15 fb^{-1}. The a_T could also be discovered simultaneously, producing a striking signal of TCSM model, but this will require more luminosity. Confirmation of the origin of the resonances could then be obtained from their expected characteristic decay angular distributions.

5 Acknowledgments

This work has been performed within the ATLAS Collaboration, and we thank collaboration members for helpful discussions. We have also made use of the physics analysis framework and tools which are the result of collaboration-wide efforts.

References

[1] Chanowitz, Michael S., , , Presented at the 23rd International Conference on High Energy Physics, Berkeley, Calif., Jul 16-23, 1986.

[2] Weinberg, Steven, Phys. Rev. **D19** (1979) 1277–1280.

[3] Susskind, Leonard, Phys. Rev. **D20** (1979) 2619–2625.

[4] Holdom, Bob, Phys. Rev. **D24** (1981) 1441.

[5] Appelquist, Thomas W. and Karabali, Dimitra and Wijewardhana, L. C. R., Phys. Rev. Lett. **57** (1986) 957.

[6] Yamawaki, Koichi and Bando, Masako and Matumoto, Ken-iti, Phys. Rev. Lett. **56** (1986) 1335.

[7] Akiba, T. and Yanagida, T., Phys. Lett. **B169** (1986) 432.

[8] Eichten, Estia and Lane, Kenneth D., Phys. Lett. **B90** (1980) 125–130.

[9] Lane, Kenneth, (2002).

[10] Hill, Christopher T. and Simmons, Elizabeth H., Physics Reports **381** (2003) 235–402.

[11] Lane, Kenneth D. and Eichten, Estia, Phys. Lett. **B222** (1989) 274.

[12] Eichten, Estia and Lane, Kenneth D., Phys. Lett. **B388** (1996) 803–807.

[13] Eichten, Estia and Lane, Kenneth D. and Womersley, John, Phys. Lett. **B405** (1997) 305–311.

[14] Hill, Christopher T., Phys. Lett. **B345** (1995) 483–489.

[15] Lane, Kenneth D., (1993).

[16] Lane, Kenneth D., (1994).

[17] Peskin, Michael E. and Takeuchi, Tatsu, Phys. Rev. Lett. **65** (1990) 964–967.

[18] Golden, Mitchell and Randall, Lisa, Nucl. Phys. **B361** (1991) 3–23.

[19] Holdom, B. and Terning, J., Phys. Lett. **B247** (1990) 88–92.

[20] Altarelli, Guido and Barbieri, Riccardo and Jadach, S., Nucl. Phys. **B369** (1992) 3–32.

[21] Appelquist, Thomas and Sannino, Francesco, Phys. Rev. **D59** (1999) 067702.

[22] Knecht, Marc and de Rafael, Eduardo, Phys. Lett. **B424** (1998) 335–342.

[23] Hirn, Johannes and Sanz, Veronica, (2006).

[24] Eichten, Estia and Lane, Kenneth, (2007).

[25] Lane, Kenneth D., Phys. Rev. **D60** (1999) 075007.

[26] Lane, Kenneth and Mrenna, Stephen, Phys. Rev. **D67** (2003) 115011.

[27] Sjostrand, Torbjorn and Mrenna, Stephen and Skands, Peter, JHEP **05** (2006) 026.

[28] Mrenna, S., Private communication.

[29] Kersevan, Borut Paul and Richter-Was, Elzbieta, hep-ph/0405247 (2004).

[30] Alwall, Johan and others, JHEP **09** (2007) 028.

[31] Richter-Was E., Froidevaux D., Poggioli L., ATLAS note, ATL-PHYS-98-131 (1998).

[32] S. Dean and P. Sherwood, http://www.hep.ucl.ac.uk/atlas/atlfast.